NASA Technical Memorandum 4771

Thrust Vectoring on the NASA F-18 High Alpha Research Vehicle

Albion H. Bowers and Joseph W. Pahle

November 1996

NASA Technical Memorandum 4771

Thrust Vectoring on the NASA F-18 High Alpha Research Vehicle

Albion H. Bowers and Joseph W. Pahle
Dryden Flight Research Center
Edwards, California

National Aeronautics and
Space Administration

Office of Management

Scientific and Technical
Information Program

1996

THRUST VECTORING ON THE NASA F-18 HIGH ALPHA RESEARCH VEHICLE

Albion H. Bowers
Joseph W. Pahle
NASA Dryden Flight Research Center
Edwards, CA

ABSTRACT

Investigations into a multiaxis thrust-vectoring system have been conducted on an F-18 configuration. These investigations include ground-based scale-model tests, ground-based full-scale testing, and flight testing. This thrust-vectoring system has been tested on the NASA F-18 High Alpha Research Vehicle (HARV). The system provides thrust vectoring in pitch and yaw axes. Ground-based subscale test data have been gathered as background to the flight phase of the program. Tests investigated aerodynamic interaction and vane control effectiveness. The ground-based full-scale data were gathered from static engine runs with image analysis to determine relative thrust-vectoring effectiveness. Flight tests have been conducted at the NASA Dryden Flight Research Center. Parameter identification input techniques have been developed. Individual vanes were not directly controlled because of a mixer-predictor function built into the flight control laws. Combined effects of the vanes have been measured in flight and compared to combined effects of the vanes as predicted by the cold-jet test data. Very good agreement has been found in the linearized effectiveness derivatives.

NOMENCLATURE

Axial	total axial force, lbf
b	span, ft
c	reference chord, ft
C_{dpv}	linearized pitch vane effectiveness
C_{dyv}	linearized yaw vane effectiveness
$C_{A_{aero}}$	aerodynamic axial force coefficient
$C_{D_{aero}}$	aerodynamic drag force coefficient
C_L	aerodynamic lift force coefficient
C_l	aerodynamic rolling moment coefficient
C_m	pitching moment
$C_{m_{aero}}$	aerodynamic pitching moment coefficient

$C_{N_{aero}}$	aerodynamic normal force coefficient
$C_{n_{aero}}$	aerodynamic yawing moment coefficient
C_t	thrust force coefficient
$C_{Y_{aero}}$	aerodynamic side force coefficient
d1	upper left vane deflection, deg
d2	outer left vane deflection, deg
d3	lower left vane deflection, deg
d4	upper right vane deflection, deg
d5	outer right vane deflection, deg
d6	lower right vane deflection, deg
dpv	generalized average pitch vanes deflection, deg
dyv	generalized average yaw vanes deflection, deg
F_{np}	net propulsive force, lbf
$f(x)$	arbitrary function of variable x
HARV	High Alpha Research Vehicle
l	length of moment arm from center of gravity to vanes, ft
Lift	total lift force, lbf
NASA	National Aeronautics and Space Administration
Normal	total normal force, lbf
NPR	nozzle pressure ratio, p_t / p_∞
p_t	jet total pressure, lbf/ft^2
p_∞	ambient pressure, lbf/ft^2
pitch	total pitching moment, ft·lbf
RFCS	research flight control system
roll	total roll moment, ft/lbf
S	reference area, ft^2
Side	total side force, lbf
TVCS	thrust-vectoring control system
v	velocity, ft/sec
$vane\ 2_{angle}$	radial vane angle for vane 2, deg
$vane\ 3_{angle}$	radial vane angle for vane 3, deg

yaw	total yaw moment, ft/lbf
α	angle of attack, deg
β	angle of side slip, deg
δ_a	aileron deflection, deg
δ_e	elevator deflection, deg
$\delta_{j_{rms}}$	jet-turning angle, deg
δ_{lef}	leading-edge flap deflection, deg
δ_r	rudder deflection, deg
δ_{tef}	trailing-edge flap deflection, deg
δ_v	vane deflection, deg
ρ	density of air, slug/ft^3

INTRODUCTION

A strong interest in thrust vectoring[1,2] has led to many experiments designed to incorporate thrust vectoring into current- and next-generation aircraft. Most of these studies have focused on vectoring in the pitch plane to improve the pitch control power[3,4] or in the yaw plane to improve yaw control power. [5–7] Some studies have examined vectoring in the pitch and yaw planes.[8–10]

To date, only a few research aircraft have flown with the capability of vectoring in both pitch and yaw. Two of these aircraft have completed research programs using axisymmetric nozzles with postexit vanes for thrust vectoring. These two aircraft are the U. S. Navy X-31A[11] and the NASA F-18 High Alpha Research Vehicle (HARV) with a thrust-vectoring control system (TVCS) installed.[12–15] Based on previous developmental tests,[8] both aircraft selected thrust-vectoring systems that employed three postexit vanes radially displaced about their axisymmetric nozzles.

Early information was required to properly characterize an axisymmetric nozzle with postexit exhaust vanes like that applied to the NASA F-18 HARV. These data were provided by testing ground-based models of the F-18 HARV with the TVCS installed. Two aerodynamic interaction tests were performed at the NASA Langley Research Center. The first test was conducted in the Full-Scale Facility 30- by 60-ft wind tunnel. The test characterized the aerodynamic interaction effects on a full-configuration, 16 percent–scale F/A-18 model that were caused by vectoring the exhaust plume at low speeds.[16] The second test was conducted in the 16-Ft Transonic Tunnel using a wingtip-supported 10 percent–scale F/A-18 model. This test was conducted between Mach 0.3 and 0.7 and angles of attack between 0° and 70°, with military-power and full-afterburner nozzles at nozzle pressure ratios (NPRs) between 1.0 and 5.0,[17] to further examine aerodynamic interaction effects caused by vectoring the exhaust plume.

A static cold-jet test was also conducted at the NASA Langley 16-Ft Transonic Tunnel to characterize the thrust-turning effectiveness of the postexit vanes on a 14.25 percent–scale nozzle

model.[18,19] This test was only of the nozzle and modeled only the internal flow of the nozzle and the vanes.

A static ground test, called the “hot loads” test, was conducted with the aircraft after the TVCS had been installed at the NASA Dryden Flight Research Center. The aircraft was secured to the Edwards Air Force Base Universal Horizontal Thrust Stand. The thrust stand was only capable of resolving forces in the axial direction, and comparisons of these results with the cold-jet test axial thrust loss data were made.[19] Infrared images of the exhaust flow were used to estimate plume-deflection angles. Hot loads test plume-deflection infrared estimates were also compared to cold-jet test results.

Flight tests were also conducted at NASA Dryden. In-flight plume deflection is difficult to measure directly, so indirect methods to estimate thrust-vectoring effectiveness were used.[20–22] Parameter identification input techniques were developed,[23] both pilot-flown and preprogrammed through the use of an on-board excitation system that controlled the postexit vanes. Individual vanes were not directly controlled because of a mixer-predictor function built into the flight control laws. As such, combined effects of the vanes were measured in flight and compared to combined effects of the vanes as predicted by the cold-jet test data.

This paper presents an overview of the ground-based tests, results of the infrared data of the hot loads test of the installed TVCS, and estimates of the effectiveness of the TVCS from in-flight parameter identification. These full-scale results are compared to the subscale tests. All tests of this system are now complete, and this report summarizes significant results of the full-scale tests in comparison to predicted thrust-vectoring control effectiveness.

HIGH ALPHA RESEARCH VEHICLE DESCRIPTION

The F-18 HARV is a high-performance twin-turbofan jet engine fighter-attack airplane built by McDonnell Douglas Aerospace (St. Louis, Missouri) (fig. 1).[12–15] The HARV has midwing-configuration wings, twin vertical tails canted outwards at 20° from the vertical, midmounted horizontal tailplanes, and leading-edge extensions that run forward along the fuselage to near the canopy. The engines are General Electric (Lynn, Massachusetts) F404-GE-400 engines rated at 10,000 lbf static thrust at sea level in the full military-power setting and 16,000 lbf static thrust at sea level in the maximum-afterburner setting.

The aircraft was modified by the addition of a rudimentary TVCS that uses three postexit vanes around each engine. The geometry of the TVCS hardware uses three vanes mounted around each engine of the F-18 airplane. Vanes replace the standard divergent section of the nozzle and external flaps. The convergent section of the nozzle remains on the aircraft. The vanes were designed to be stowed at –10°, out of the exhaust plume. During vectoring maneuvers, a maximum of two vanes on any one engine were commanded in contact with the flow at one time, helping to alleviate thermal and load constraints on the vane system.

The thrust-vectoring vanes were controlled through use of modified flight control computers that allowed the basic flight control laws to be bypassed with research flight control laws in a

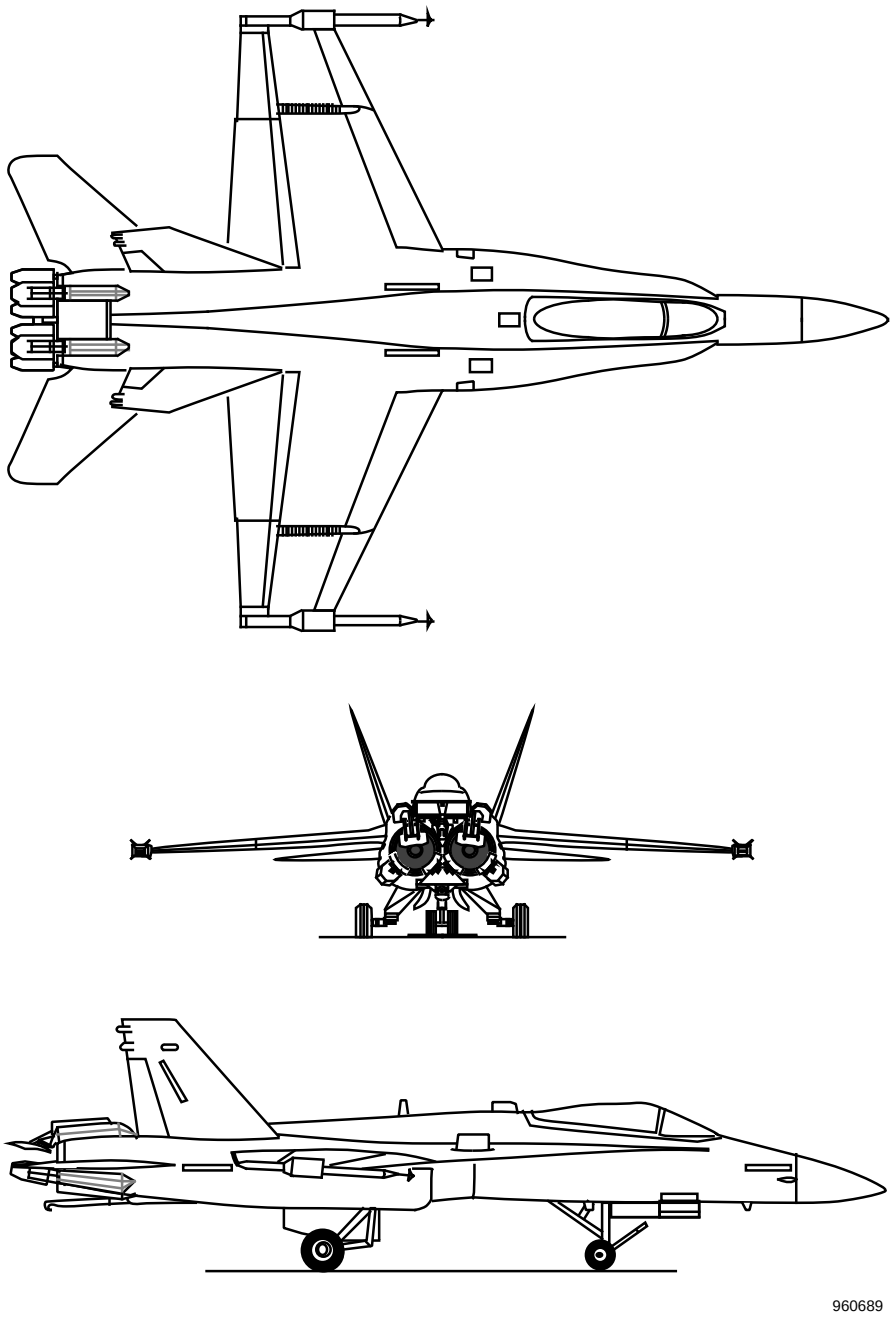

Figure 1. Three-view drawing of the F-18 HARV.

portion of the flight control computers called the research flight control system (RFCS). The RFCS envelope of the aircraft was Mach 0.2–0.7 and initial altitudes of 15,000–35,000 ft, which was later expanded to 45,000 ft. The basic F-18 flight control laws resided in the 701E (General Electric, Lynn, Massachusetts) portion of the flight control computers and passed data back and forth to the RFCS.

The output of the control laws was a simple command of pitch or yaw vectoring moments. To make use of these commanded moments from the thrust vectoring, a schedule was devised, called

the mixer-predictor or the mixer, where the pitch and yaw commands were converted into individual vane deflections. Several releases of mixer software were made, and two were carried to flight (Mixer 1 and Mixer 4.2). Mixer 1 was a cooperative effort between McDonnell Douglas Aerospace, NASA Dryden, and NASA Langley.[24] Mixer 4.2 was a cooperative design between NASA Langley and NASA Dryden.[25]

The ability to use preprogrammed maneuvers by superimposing motions over the control surface outputs, called the on-board excitation system, resided within one part of the RFCS. The ability to separate the individual control surface motions through the on-board excitation system allowed reduction in surface motion correlation and reduced uncertainty in the final effectiveness estimates.

THRUST-VECTORING CONTROL SYSTEM DESCRIPTION

Figure 2 shows the vane configuration for the left engine only. The upper-vane centerline is 5° outboard of the vertical plane. The outboard-vane centerline is 118° counterclockwise from the upper-vane centerline. The outboard-vane centerline to the lower-vane centerline measurement is 103.5° counterclockwise. The lower-vane centerline to the upper-vane centerline measurement is 138.5° counterclockwise. The upper vane was larger than the outer or lower vanes (fig. 3) because of the uneven radial spacing caused by structural considerations. The exhaust-plume side of each vane is concave, with each vane forming part of a spherical surface of 36 in. radius axially and laterally.

The total amount of turning of the jet exhaust plume, or jet-turning angle, is defined as the root mean square of the equivalent thrust-vector deflection angle in pitch and yaw as measured by the resultant force (fig. 4). The axial thrust loss for the deflected flow is defined as the loss in the

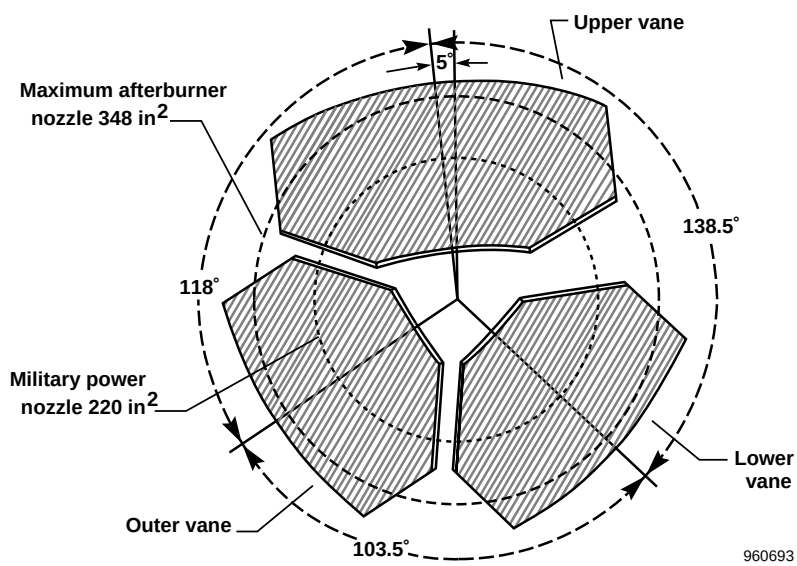

Figure 2. Thrust-vectoring control system end-view of the left engine looking forward. Radial vane included angles are displayed. All vanes shown fully extended into the plume. The right engine is a mirror image of the left.

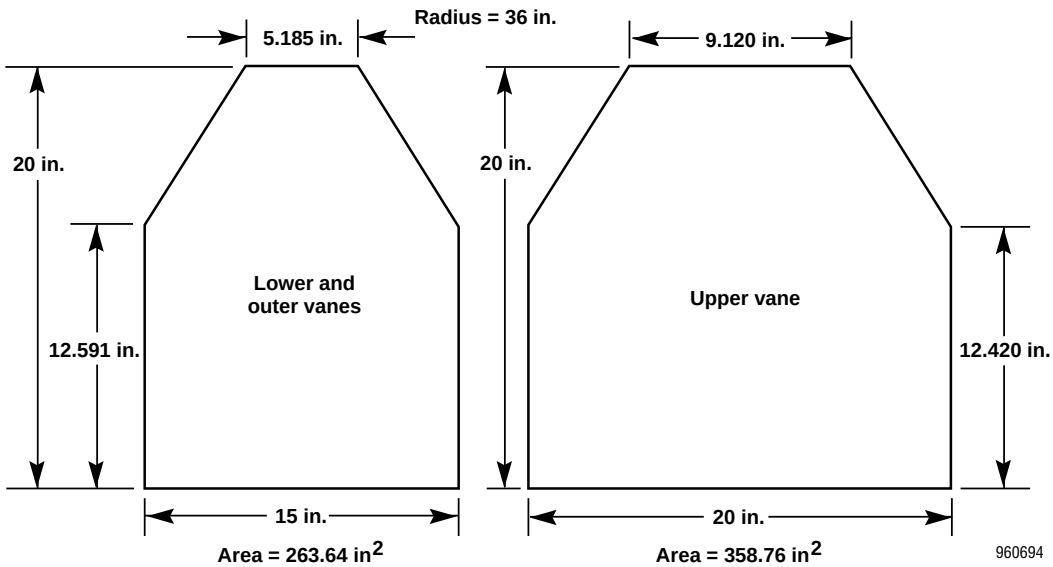

Figure 3. Dimensions for flight vanes.

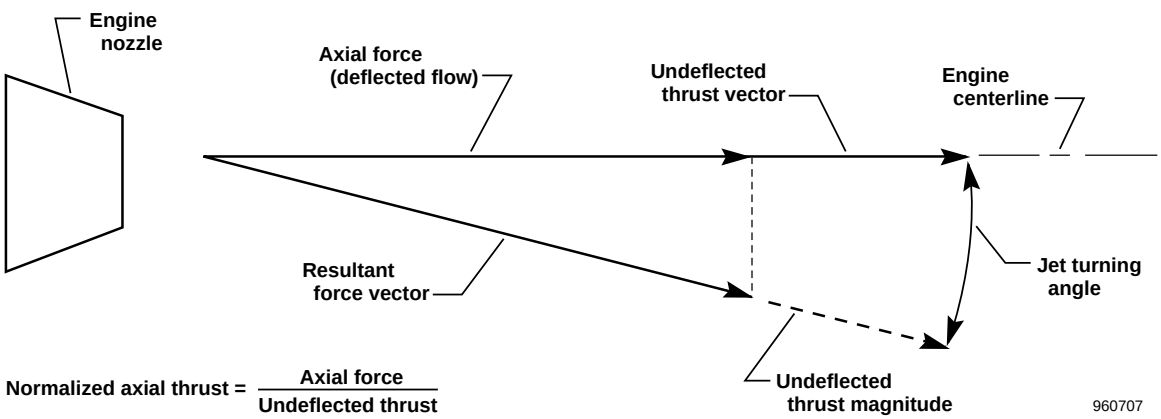

Figure 4. Schematic of jet-turning angle and axial thrust loss definitions.

thrust of the axial force when compared to the undeflected thrust. The normalized axial thrust is the absolute value of the axial force divided by the absolute value of the undeflected thrust.

TESTING AND MODELS

Several tests were conducted to characterize thrust vectoring on the F-18 HARV. These tests were two subscale aerodynamic interaction tests, one of which is discussed here; a subscale cold-jet test; a full-scale hot loads test; and the flight test (table 1).

The 16 percent–scale aerodynamic interaction model was tested in the 30- by 60-ft wind tunnel at NASA Langley.[16] This particular F/A-18 model was used because, being a free-flight model, it already had ducting for the inlets, exhausts, and high-pressure air built into the design.[4]

Table 1. Test matrix.

Test	Model	Scale	Comments
Aero[16]	F-18 HARV	16 percent	External flow, nonmetric nozzles
Aero[17]	F-18 HARV	10 percent	Internal/external flow, nonmetric wing
Cold jet[16,18]	Left nozzle	14.25 percent	Internal flow
Hot loads[19]	F-18 HARV	Full	Static ground engine run test
Flight parameter identification[23,30]	F-18 HARV	Full	Parameter identification flight test

The model, designed for use in free-flight testing, was of very light construction, which resulted in tests being conducted at low dynamic pressures to prevent structural damage. The radial location of the vanes on the model was oriented in the same way as for the aircraft. The hinges were located to allow correct vane position and deflection angles. A spin chute canister was also included in the modifications to the model. The primary difference between the aircraft and the aerodynamic interaction model configuration was the nozzle areas. The nozzles used in the aerodynamic interaction test were 13.31 in^2 in area, which corresponds to a 520-in^2 nozzle area on the full-size F-18 airplane. The tailpipe area nominally used during flight tests is 348 in^2 in the thrust-vectoring envelope. Differences between the aircraft and the low-speed aerodynamic interaction model also included AIM-9 missiles (Raytheon, Bedford, Massachusetts) in place of research airdata wingtip probes, the omission on the model of video camera fairings used on the aircraft, and the lack of incorporation on the wind-tunnel model of the horizontal stabilizer area reduction (1.6 percent in area) for thrust-vectoring fairing clearance used on the aircraft.

The 10 percent–scale test was conducted at NPRs between 1.0 and 5.0, free-stream Mach numbers between 0.3 and 0.7, and angles of attack between 0° and 70°.[17] This model was wingtip-supported and differed from the flight vehicle configuration by having faired-over inlets, nose strakes, and larger leading-edge extension slots. Significant modification was undertaken to make the 10 percent–scale F/A-18 model metric aft fuselage area geometrically resemble the HARV configuration with postexit vanes and their associated actuator fairings and the spin chute canister.

A 14.25 percent–scale model of the left exhaust nozzle with postexit vanes of the F-18 HARV aircraft was tested.[16,18] The objective of this static test was to gather a comprehensive set of data from direct jet-turning effectiveness of the postexit vanes. Data were gathered with a force and moment balance. The cold-jet test was performed in the NASA Langley 16-ft Transonic Tunnel. The comprehensive data set from the cold-jet test formed the baseline of comparison to all subsequent tests. Two nozzle sizes were used in this test. These sizes corresponded to military-power and maximum-afterburner nozzles at a nominal flight condition in the thrust-vectoring

envelope of the aircraft. The vane angles were measured with simple protractors, and their positions varied from –10° to 30° deflection (approximately 0.5° accuracy). The NPR variations were from 1.0 (no flow) to 6.0 for most test cases.

The static test of the TVCS installed on the aircraft with running engines was called the "hot loads" test. The hot loads test was the first test of the F-18 HARV with the TVCS installed and was conducted at NASA Dryden using the thrust stand at Edwards AFB. One research objective of this portion of the study was to determine the feasibility of using digitized infrared imaging as a technique to determine thrust-vectoring effectiveness. Infrared imaging provided an ability to directly compare exhaust-plume deflections to the cold-jet test ground facility predictions. With the inability to measure actual vectoring forces developed during the hot loads test, infrared imaging could offer an alternative to validate the flight hardware implementation of thrust vectoring. Test conditions of the hot loads tests included military-power, midafterburner-power (with a nozzle exit area of 56 percent), and maximum-afterburner nozzles with all combinations of single-vane and two-vane equal deflections. The aircraft was secured to the thrust stand, which could directly measure thrust loss during the test.[19]

Flight tests of the F-18 HARV were conducted at NASA Dryden. Parameter identification maneuvers were used to determine stability and control coefficients using the error output technique and pEst code.[20–22] One parameter extracted from the flight data was thrust-vectoring control effectiveness, of which some results have been reported.[23,26–28] This parameter estimation technique does not differentiate between thrust-vectoring forces and moments and the aerodynamic interactions caused by thrust vectoring. As a consequence, these two parameters are inseparable and cannot be independently identified. During the F-18 HARV flight testing of these data, however, the aerodynamic interaction was considered to be very low because of the low–dynamic pressures level-flight 1-*g* condition used during the parameter identification maneuvers. As a result, the predominant characteristic estimated is that of the thrust-vectoring effectiveness. The low–dynamic pressure data are a result of all test points being flown in 1-*g* level flight and high angle of attack confining the aircraft to relatively slow flight. Further complicating the issue is the mixer function in the flight control laws preventing individual vanes from being controlled. As a result, a collective vane function is identified, and estimates of vectoring control power from flight are made and then compared to equivalent collective vane effectiveness from the cold-jet test data.

THRUST-VECTORING RESEARCH RESULTS

The research conducted was divided into four areas. These four areas are: aerodynamic interaction tests, the static cold-jet test, the static engine run ("hot loads") test of the installed system on the aircraft, and the flight test of the aircraft.

Aerodynamic Interaction Tests

Aerodynamic interaction with thrust vectoring was an unknown; therefore, two tests were conducted to investigate aerodynamic interaction. The tests were a 16 percent–scale low-speed test with a subsonic ejector exhaust conducted in the NASA Langley 30- by 60-ft low-speed wind

tunnel and a 10 percent–scale test with a sonic nozzle conducted in the 16-ft Transonic Tunnel at NASA Langley.

Aerodynamic forces and moments on the F-18 HARV with the installed TVCS are taken at the 0.24-chord position. Vectoring direction definitions for plume deflections are as follows: up is negative, down is positive, right is negative, and left is positive. When the thrust-vectoring vanes are not installed, the nozzle configuration is defined as unvectored. For any one engine, when two vanes are deflected into the exhaust, the third vane is retracted at –10° deflection and is referred to as the retracted vane.

Significant findings of the low-speed test were that forces were mildly adverse and moments were mildly proverse. For these aerodynamic interaction tests, the plume deflections were –17° up, 14° down, and –9° right. A change in lift coefficient of approximately 0.1 caused by vectoring in the pitch plane was found over the entire angle-of-attack range (fig. 5) for the tested condition. A change in pitching moment of approximately 0.1 was found near 0° angle of attack, decreasing to 0 increment in moment near 65° angle of attack with vectoring in the pitch plane (fig. 6). Vectoring was intended primarily as a moment-producing effector, so vectoring the plume up would cause a noseup pitching moment. But the exhaust plume vectored up would decrease the lift coefficient in the adverse direction while increasing the pitching moment coefficient in the proverse direction. This behavior is analogous to a blown flap.

The 10 percent–scale test[17] was conducted to investigate aerodynamic interactions over a representative configuration. The results of the 10 percent–scale test expanded the database and supported previous conclusions of the 16 percent–scale test, in particular that substantial gains in controllability are provided by a multiaxis thrust-vectoring capability.

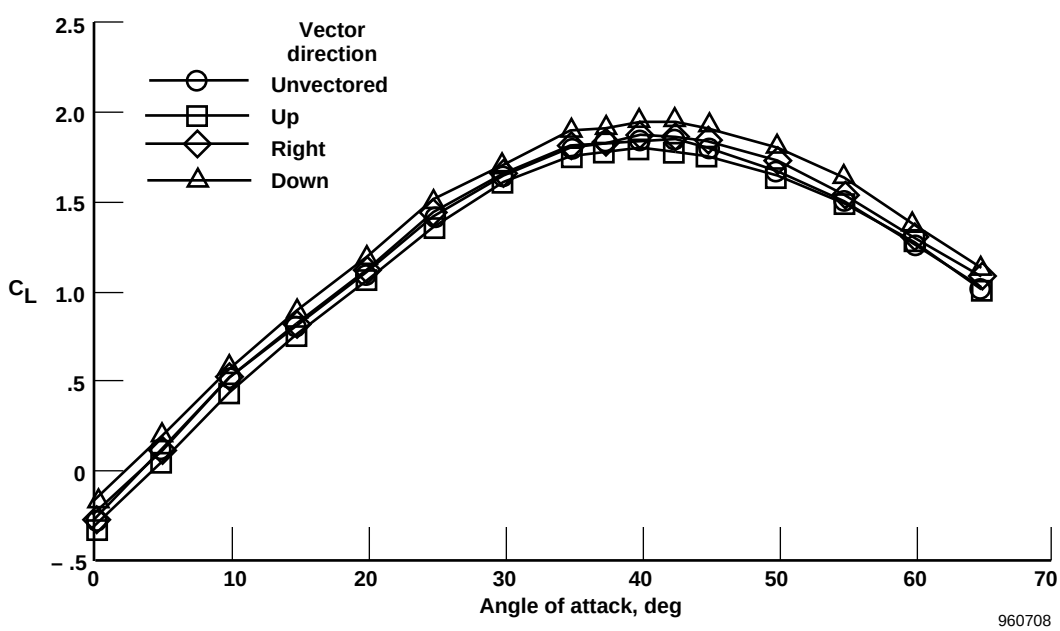

Figure 5. Pitching moment coefficient as a function of angle of attack, with thrust vectoring varying direction; $\delta_e = -12°$, $\delta_a = 0°$, $\delta_r = 0°$, and $C_t = 0.8$.

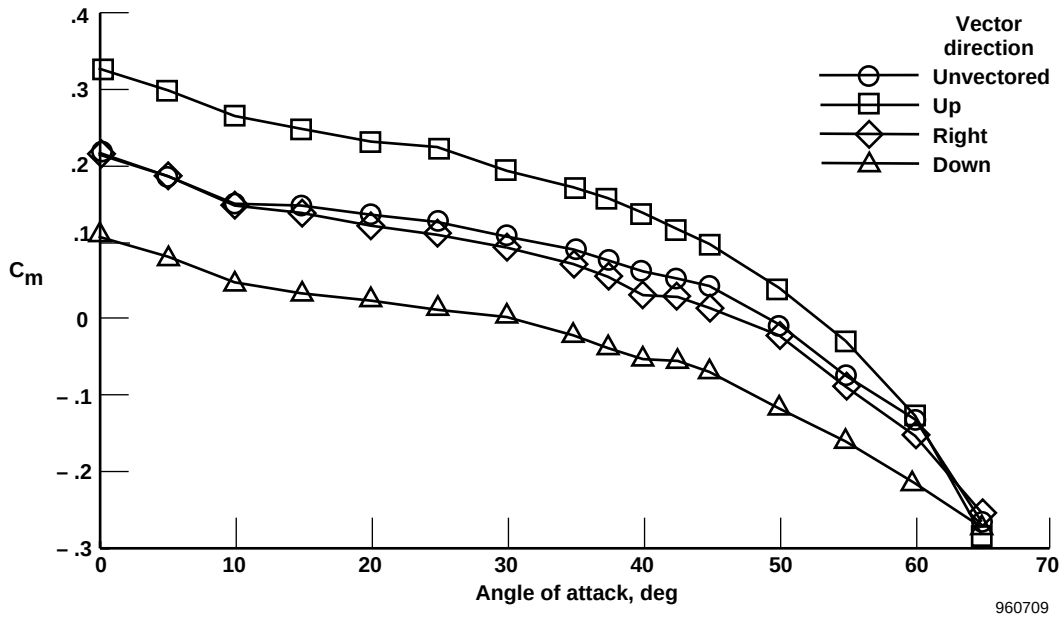

Figure 6. Pitching moment coefficient as a function of angle of attack, with thrust vectoring varying direction; $\delta_{lef} = 34°$, $\delta_{tef} = 0°$, $\delta_e = –12°$, $\delta_a = 0°$, $\delta_r = 0°$, and $C_t = 0.8$.

Thrust-Vectoring Effectiveness Tests

Although many tests were conducted to examine the effectiveness of thrust vectoring, three tests in particular are examined here. The tests in this section are the cold-jet test, the hot loads test, and the in-flight parameter identification tests.

Cold-Jet Test

The objective of the cold-jet test was to gather a comprehensive set of data of the direct jet-turning effectiveness of the postexit vanes. Data were gathered with a force and moment balance, and plume-turning angles were inferred from the force and moment data. Because of the nonaxisymmetric installation of the vanes, pitch and yaw deflection angles are not discussed; the total root mean square of the pitch and yaw vane deflections is used instead.

Control effectiveness is defined as the angle through which the exhaust plume is turned by the vanes, regardless of the ultimate forces or moments produced. This effectiveness definition is an important distinction, as the thrust available to be turned is much larger in maximum-afterburner nozzle than in military-power nozzle.

The large upper vane produced greater plume deflection than the two small (lower and outer) vanes did. In the military-power nozzle case, the large vane was 50 percent more effective than the small vanes were; and in the maximum-afterburner nozzle case, the large vane was 25 percent more effective than the small vanes. The vanes did not become effective until they impinged on

the edge of the exhaust plume at approximately 15° vane deflection for military-power nozzle and approximately 10° deflection for maximum-afterburner nozzle for the selected NPR. This vane ineffectiveness results in larger dead band for the smaller military-power nozzle than for the larger maximum-afterburner nozzle. The slopes of the vane deflection–to–plume deflection curves are also close between the two tested nozzles, with the military-power nozzle having a slightly larger slope than the maximum-afterburner nozzle.

Also as expected, the NPR largely affects effectiveness. As the exhaust plume expansion increases with increased NPR, the vanes become effective at decreased vane deflections (fig. 9). The slope of the various curves are relatively insensitive to NPR variation in the 15°–20° vane deflection region. These data are for all single-vane deflections with the military-power nozzle at an NPR of 2.

Two vanes used simultaneously show greater effectiveness (fig. 10) for the same deflection when compared with single vanes (fig. 7). Effectiveness increased to approximately 100 percent in this case. Also, two vanes radially spaced closer together (fig. 3) show greater effectiveness than vanes spaced further apart. This difference could be explained by flow “leaking” through the gap between vanes, and a smaller gap will leak less. The lower and upper vanes (138.5° radial spacing (fig. 3)) were less effective than the lower and outer vanes (118° radial spacing (fig. 3)). Cold-jet test results determined that vane spacing is a very strong and important parameter, more important than vane size. These data are for the military-power nozzle at an NPR of 2.

Axial force loss was another measurement of the cold-jet test. Axial force loss data are normalized axial thrust. In all cases, increases in vane deflection caused greater axial force loss (fig. 11). In this sample case of single-vane deflections, the large upper vane caused the lowest normalized axial force (0.82) at 30° vane deflection, with the two equally sized vanes producing equal amounts of thrust loss (0.87) within experimental error. These results are for the military-power nozzle case with an NPR of 2.

The extreme edge of the plume-deflection envelope in pitch and yaw is shown with variation in NPR (fig. 12) for the maximum-afterburner nozzle for vane deflections of 30°. The extreme envelope is found by holding at least one vane at 30° deflection and at least one other vane at –10°. Retracted vane interference effects can be observed at three of the corners, near pitch and yaw coordinates (11, 9), (–25, –3), and (16, –20). The loss of turning effectiveness caused by increasing NPR is most evident near these corners, especially near coordinate (11, 9) in pitch and yaw. The other three corners, (18, –3), (–7, –10) and (–9, 9), are single-vane deflection corners and show no retracted vane interference effects. The data shown are for the left engine only and display the actual pitch and yaw plume-deflection angles, not the plume-deflection angle to the centerline as previously shown (figs. 7 to 11).

Full-Scale Static Thrust Test Infrared Data

Infrared imaging can visualize the hot exhaust plume of a jet engine. Infrared intensity is related to temperature, although in a nonlinear function. The infrared representation of the exhaust plumes, however, could be digitized and treated mathematically to calculate plume deflections. Reducing the data obtained during hot loads testing to simple digital values with no mention of infrared intensity or wavelength and circumventing classification of the results was possible. The fundamental assumption is that the infrared intensity and the plume profiles are equivalent.

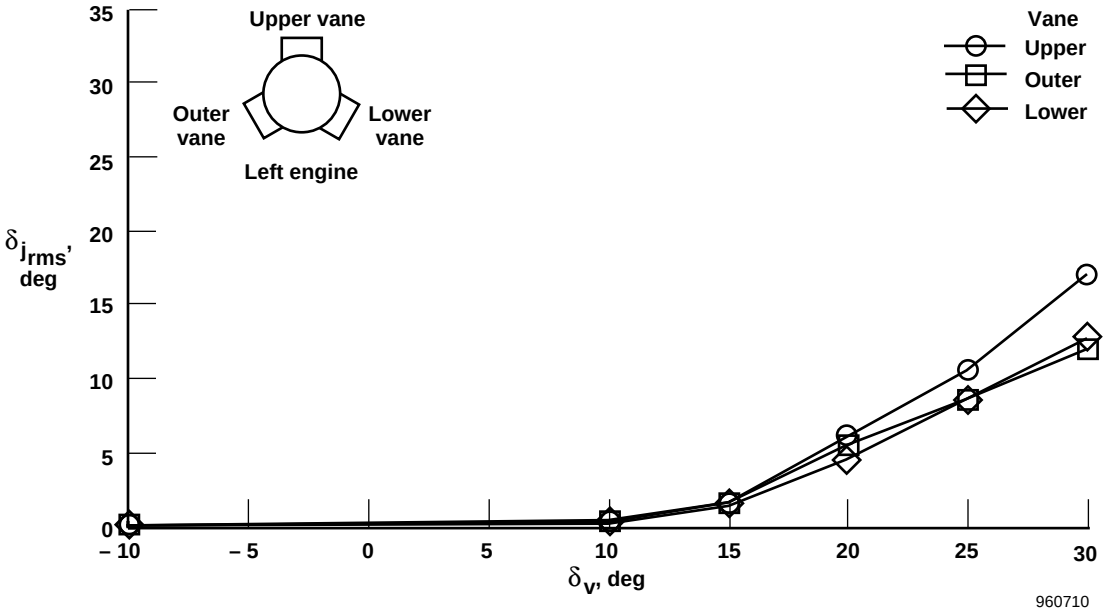

Figure 7. Jet-turning angle as a function of single-vane deflection for all three vanes with the military-power nozzle and NPR = 2.

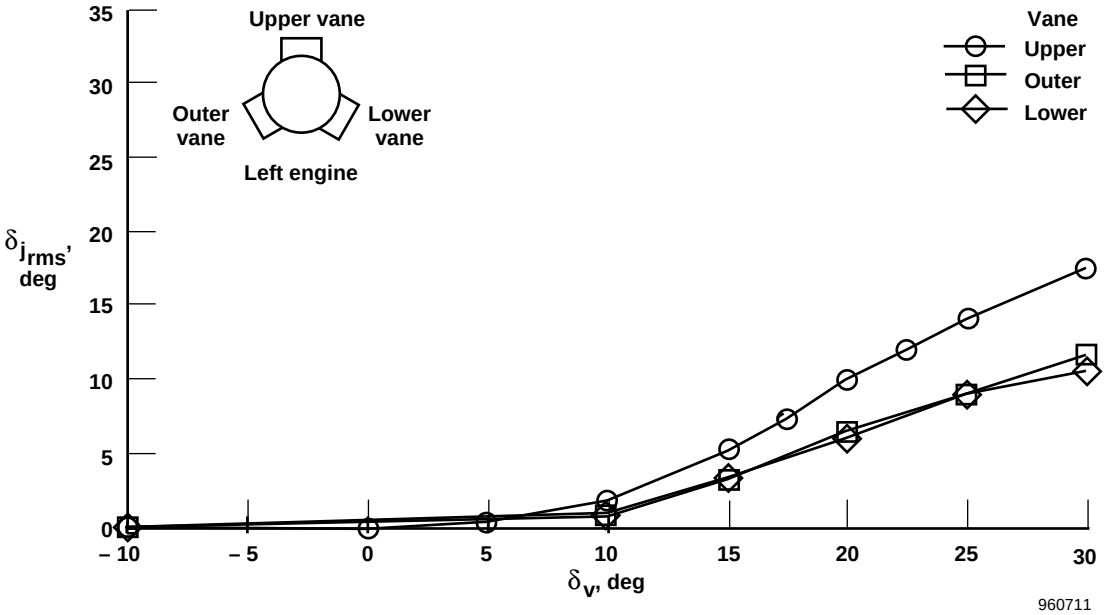

Figure 8. Jet-turning angle as a function of single-vane deflection for all three vanes with the maximum-afterburner nozzle and NPR = 2.

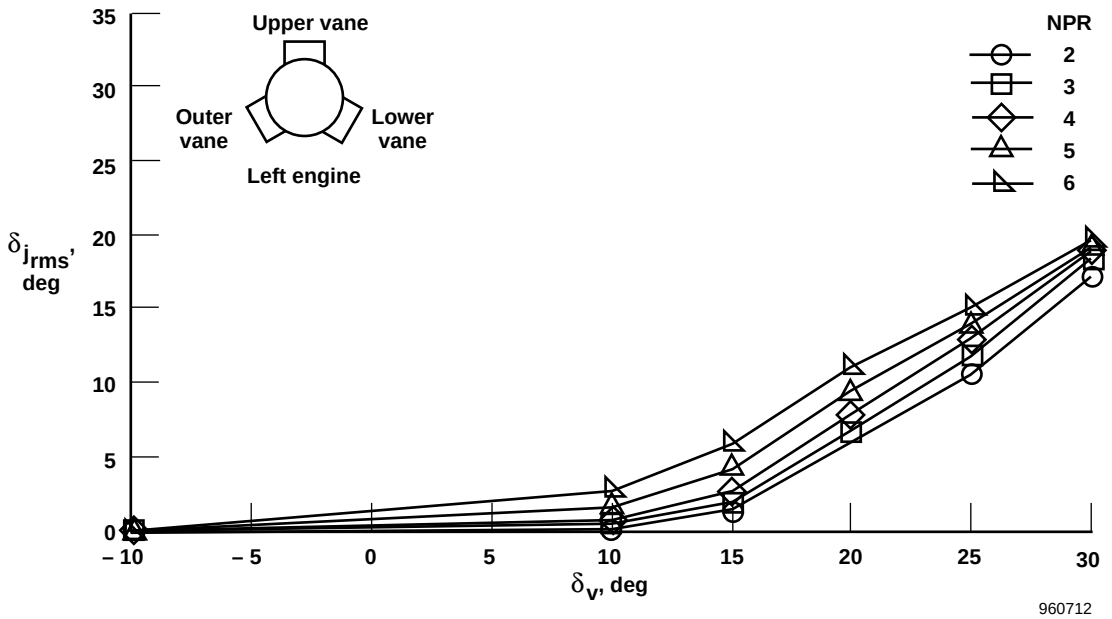

Figure 9. Jet-turning angle as a function of single-vane deflection (upper) and varying NPR with the military-power nozzle.

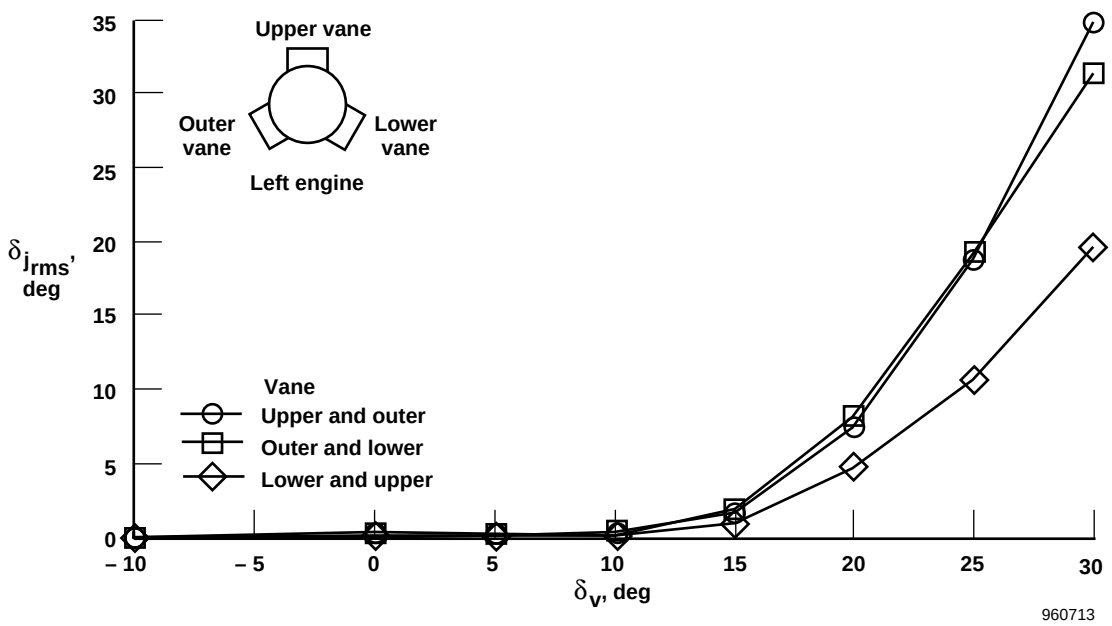

Figure 10. Jet-turning angle as a function of two-angle equal deflections for all two-vane combinations with the military-power nozzle and NPR = 2.

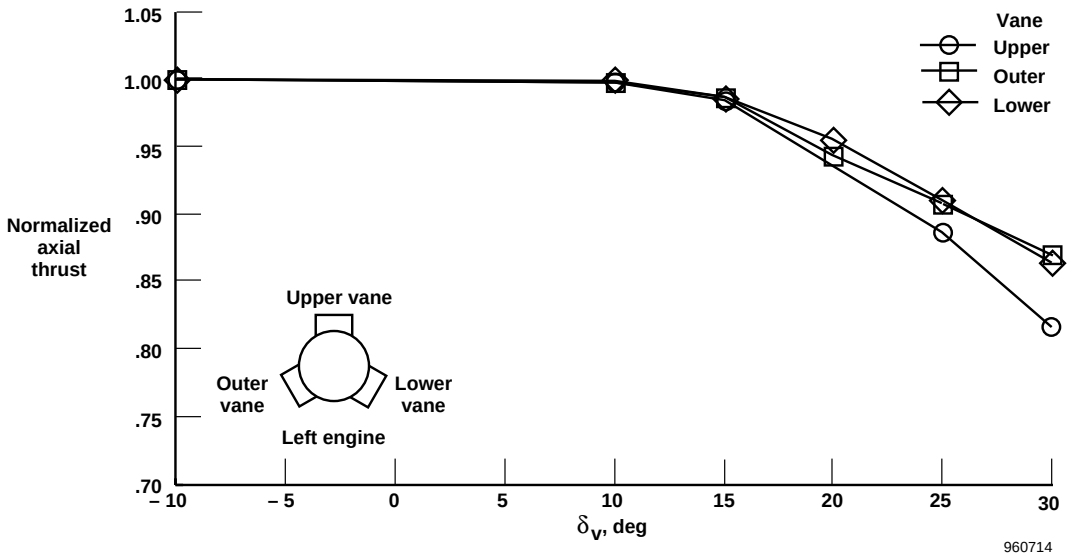

Figure 11. Normalized axial force thrust loss as a function of vane deflection angle for all single-vane deflections with the military-power nozzle and NPR = 2.

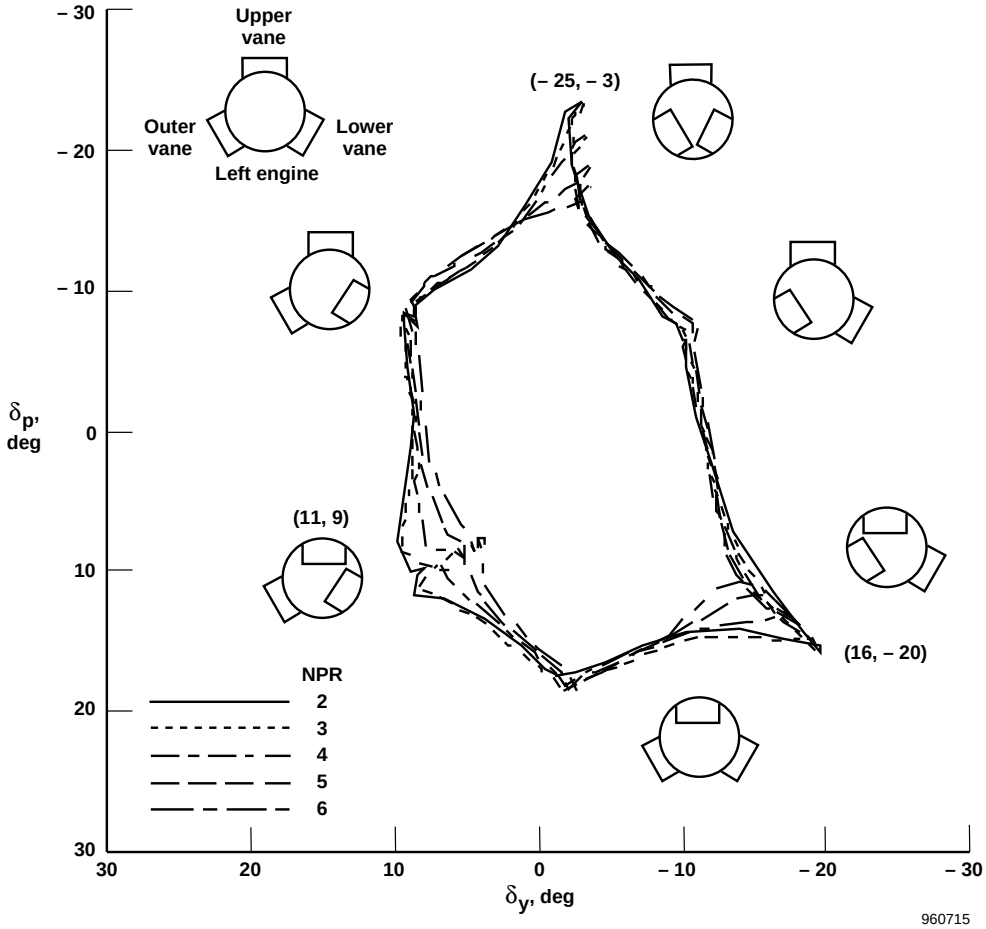

Figure 12. Maximum jet-turning angle envelope, in pitch and yaw, where at least one vane is deflected 30°. Maximum-afterburner nozzle and varying NPR showing retracted vane interference near corners with two-vane equal deflections. Symbols omitted for clarity.

Limitations of this technique are that the data are only two-dimensional. Geometric setup of the camera was carefully aligned with the plane of the exhaust nozzles and the exhaust plumes so that metric data could be made from the infrared data. An additional limitation is that in cases where multiple plumes exist, reconciling the resultant from the individual plumes is difficult.

Five test conditions were selected. These test conditions were: lower-vane deflection variations in military power, lower-vane deflection variations in midafterburner power (a nozzle exit area of 56 percent), upper-vane deflection variations at maximum afterburner, equal lower- and outer-vane deflection variations at military power, and equal lower- and outer-vane deflection variations at midafterburner power.

The process to gather data and analyze each test condition was as follows: only one engine was active in each test, and the other engine was at idle. The idle condition resulted in no significant signature in the final images, so no attempt was made to subtract the idle plume from the image. Some background data did exist, however, which tended to bias results to the middle of the image. This background was removed by simply setting an artificially high threshold just above the level of the background. This background is actual signal and not noise in the data. Noise within the infrared data was not a problem. Typical variations that could be ascribed to noise were much lower than the level of the signal, with the signal-to-noise ratio being approximately 50:1. Approximately 5 sec of stabilized data were recorded at each test point, resulting in approximately 63 frames of data. These 63 data sets were averaged for the final analysis.

After capturing the digital data, the data were converted to an alphanumeric format that could be easily manipulated. The format corresponded to rows and columns of the pixels from the captured data (fig. 13). (“Row” and “column” refer to the alphanumeric representation of the data manipulation and not to the physical geometric presentation of the pixels if the data were reassembled to make a photographic image as in the figure.) By examining each column and row

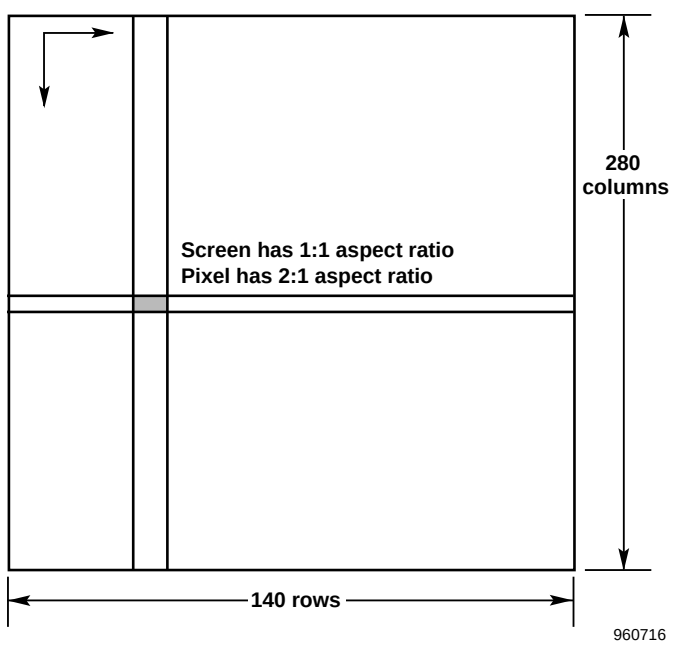

Figure 13. The layout of the rows and columns in one frame of infrared data.

individually, curves of infrared intensity were generated. Routines were constructed to integrate the areas under the curves and provide weighted averages of the curves. Simple calculations provided the centroid of each area corresponding to the representative column. Plotting these columns gives a graphical representation of the exhaust plume infrared intensity curves and the plume distribution (fig. 14). Comparing centroids of individual plume curves with vane deflection to centroids of undeflected plumes provides a direct measurement of the plume-deflection angle.

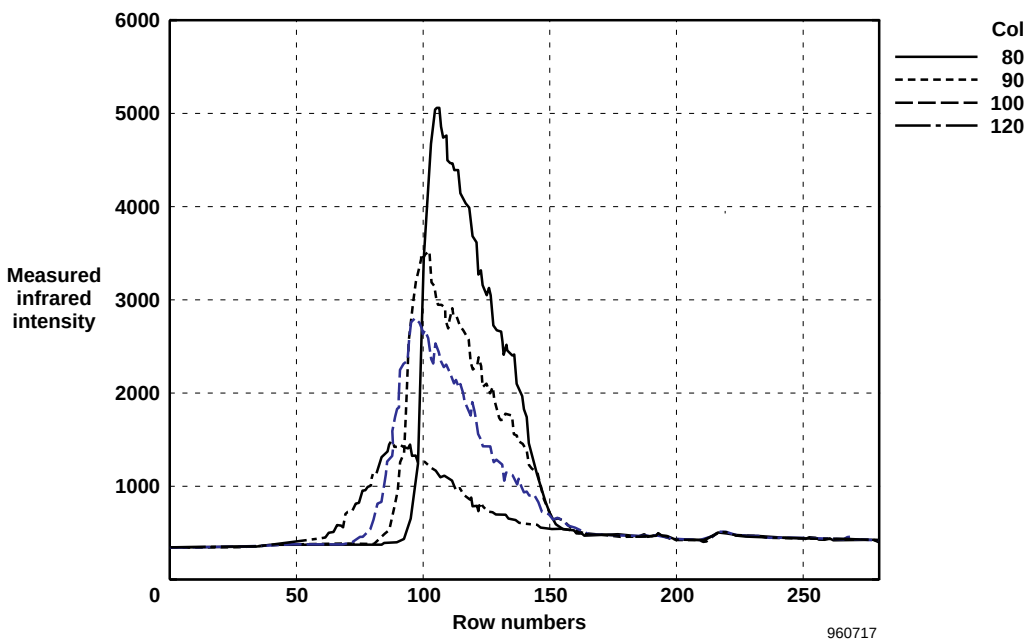

Figure 14. Typical distributions of infrared intensity in vertical sections of one frame of data.

A trapezoidal integration was applied to each column of pixels to find the area under each curve. The area of each trapezoid is given as:

$$\int_{x_i}^{x_{i+1}} f(x)\mathrm{dx} \doteq \frac{f(x_i) + f(x_{i+1})}{2}(\Delta x) = \frac{\Delta x}{2}(f_i + f_{i+1}) \tag{1}$$

Because each vertical column of pixels is exactly the same width, the calculation is given as:

$$\int_{x_1}^{x_n} f(x)\mathrm{dx} \doteq \sum_{i=1}^{n} \frac{\Delta x}{2}(f_i + f_{i+1}) \tag{2}$$

When the centroid of each area is found, it is stored as the centroid of that column. Each column is treated likewise, and the complete figure of geometric plume centroids can be plotted for each vane deflection case (fig. 15). The low or negative vane deflections with small variations in plume deflection show little or no potential effectiveness.

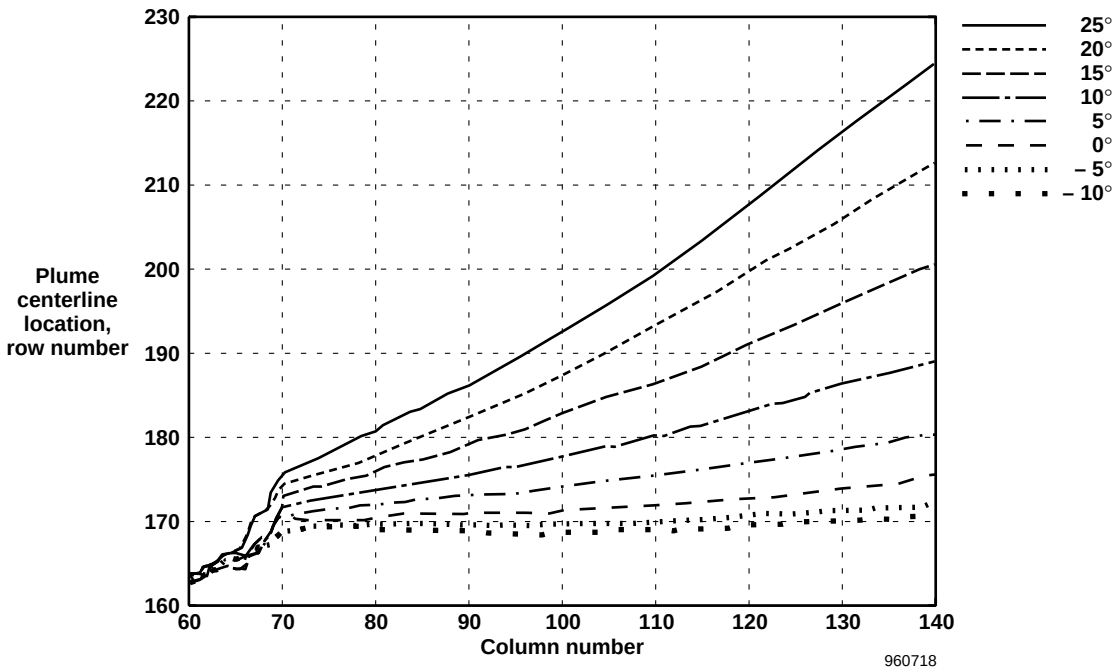

Figure 15. Typical plot of the loci of the centroids of vertical sections of data, or calculated plume centerlines.

Assuming the locus of centroids is equal to the theoretical plume centerline gives the deflection angles. Using the raw loci in such a manner and plotting them was referred to as the one-region technique.

The one-region technique was modified by considering the area above and below the centerline of the nondeflected plume as separate areas. Weighted averages of the two areas were made to determine the mean plume centerline when the plume was split, as in two-vane deflection cases. This second method was called the two-region technique. The two-region technique was developed to handle the complex flow structures resulting from two-vane equal deflections into the flow. In these cases, large secondary jets were found, and the results of the one-region technique were poor. As the geometric setup of the infrared system could only measure angles in pitch only, the plume was assumed to move in the line of action directly opposite to the vane radial angle. By using this assumption, the angle of the plume could be estimated in yaw.

Comparison of hot loads test infrared data with the NASA Langley cold-jet test data shows varying correlations for many conditions. Examples are for the lower-vane deflection with military-power nozzle (fig. 16), lower-vane deflection with midafterburner-power nozzle (fig. 17), upper-vane deflection with maximum-afterburner nozzle (fig. 18), lower- and outer-vane deflections with military-power nozzle (fig. 19), and lower- and outer-vane deflections with midafterburner-power nozzle (fig. 20).

Differences between the two analysis techniques, one-region and two-region, were small for lower-vane deflection in military-power setting (fig. 16) and were larger for midafterburner-power setting (fig. 17). The two techniques did produce varying results. Military-power setting and

single-vane deflection worked well with the one-region method when compared to the cold-jet test results (fig. 16). In the midafterburner-power with two-vane deflection case, the one-region method also seemed to match the cold-jet test data better, within 2° for most of the range (fig. 20). The two-region method seemed to match cold-jet test data best with the midafterburner-power setting and single-vane deflection (fig. 17), although not as well as a single vane in military power. And in the case of military power with two vanes, most of the operating region of the cold-jet test data is matched better by the two-region technique (fig. 19). Trends in each of these cases are well defined and correlate well, but absolute values of plume turning–effectiveness results are mixed.

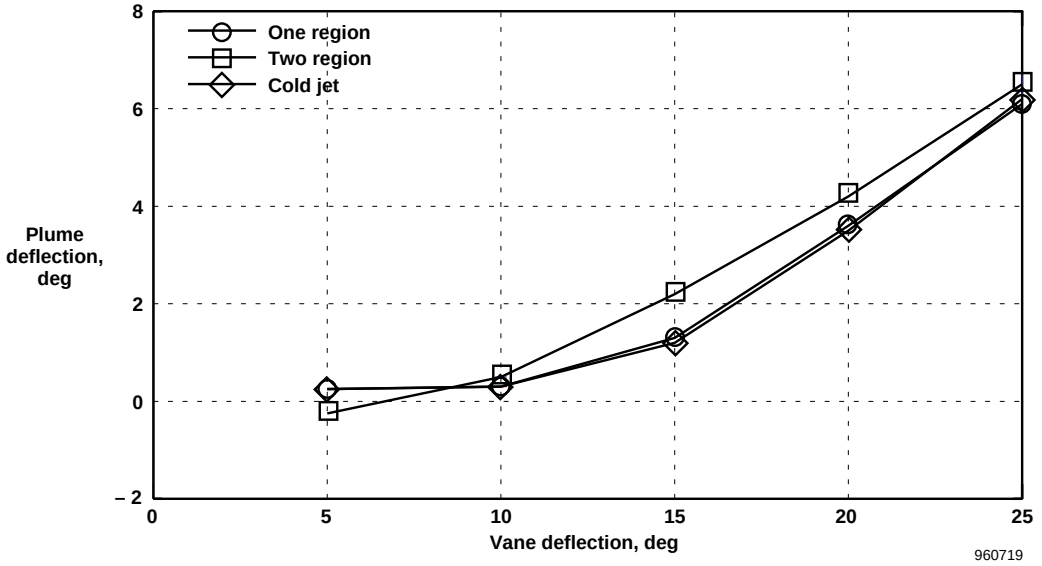

Figure 16. Lower vane deflection with nozzle in military power for one-region and two-region infrared compared with cold-jet test data.

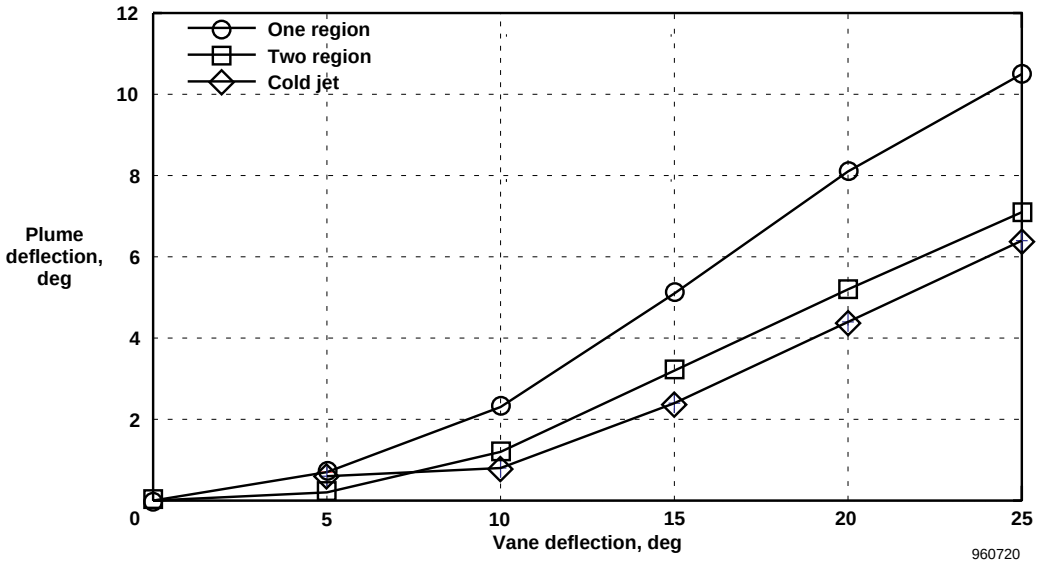

Figure 17. Lower vane deflection with nozzle in midafterburner for one-region and two-region infrared compared with cold-jet test data.

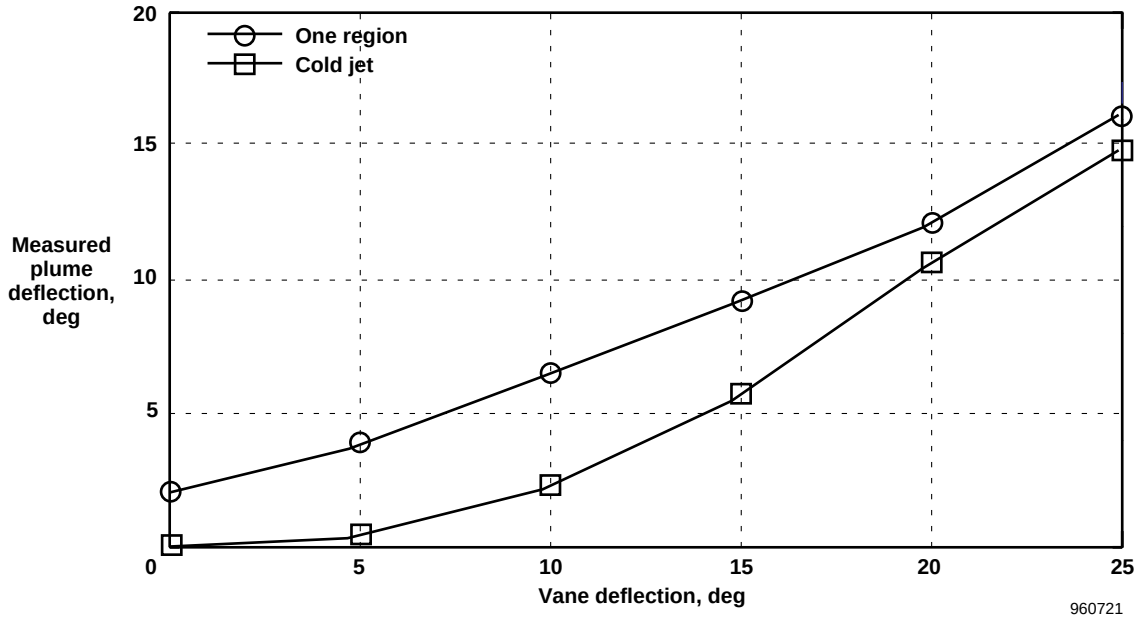

Figure 18. Upper vane deflection with nozzle in maximum afterburner for one-region infrared compared to cold-jet test data.

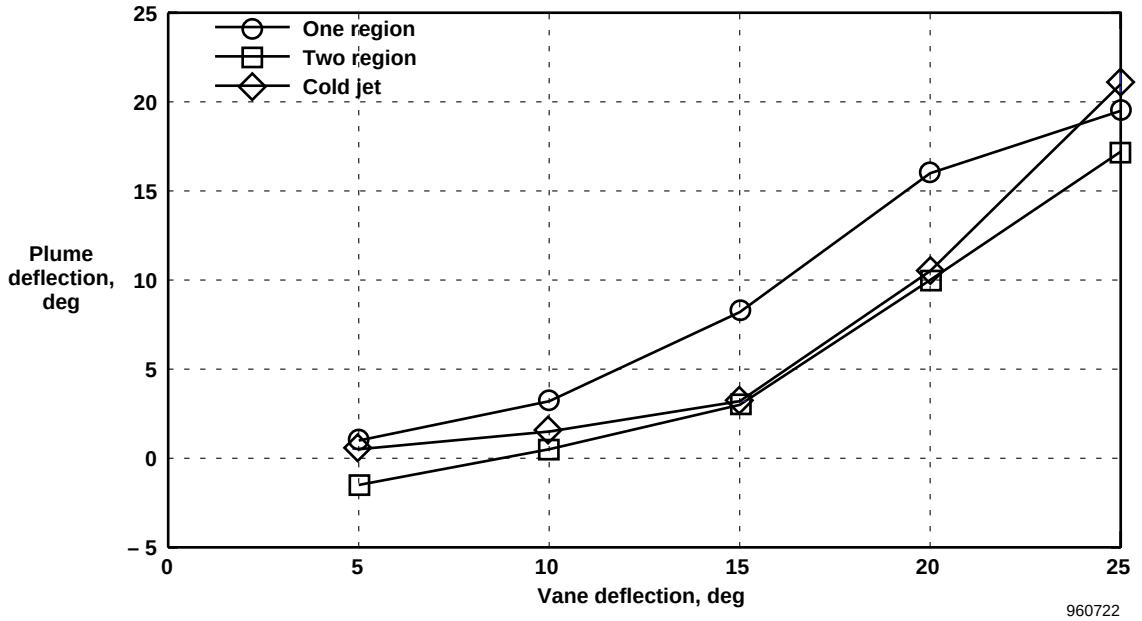

Figure 19. Lower and outer vanes deflected together with military-power nozzle for one- and two-region infrared compared with cold-jet test data.

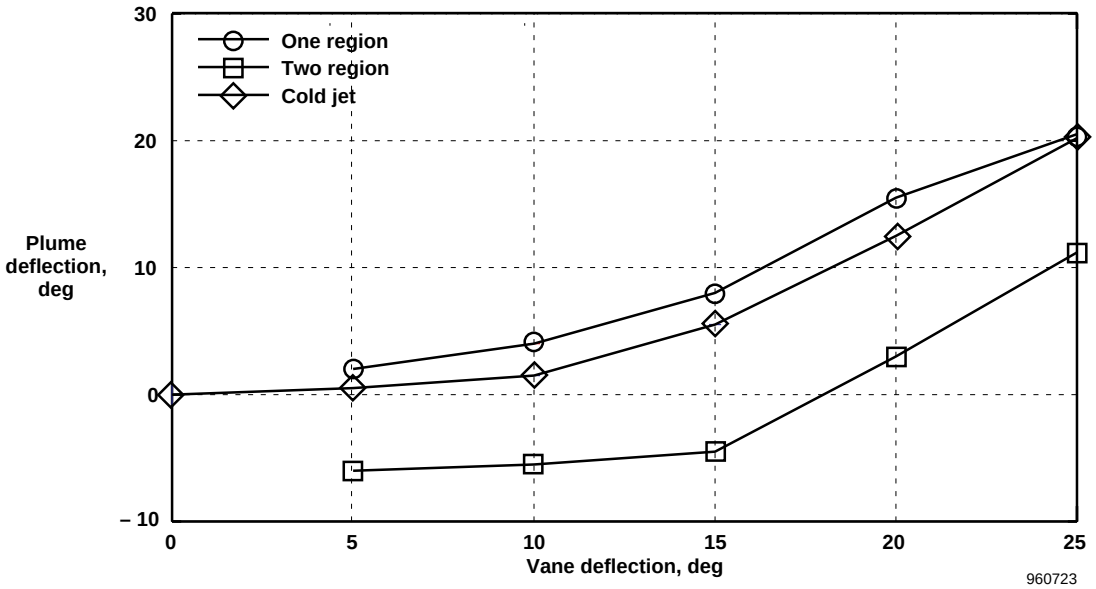

Figure 20. Lower and outer vanes deflected together with midafterburner nozzle for one- and two-region infrared compared to cold-jet test data.

Axial force, or thrust, was the only parameter for which direct measurement could be made during the hot loads tests. The thrust stand at Edwards AFB is a single-component stand and measures axial force only. These axial force results showed excellent prediction (fig. 21) and very close agreement of absolute values of thrust loss, with less than 4-percent error in thrust between the cold-jet test and the thrust-stand test data.[19] These data are for the maximum-afterburner nozzle.

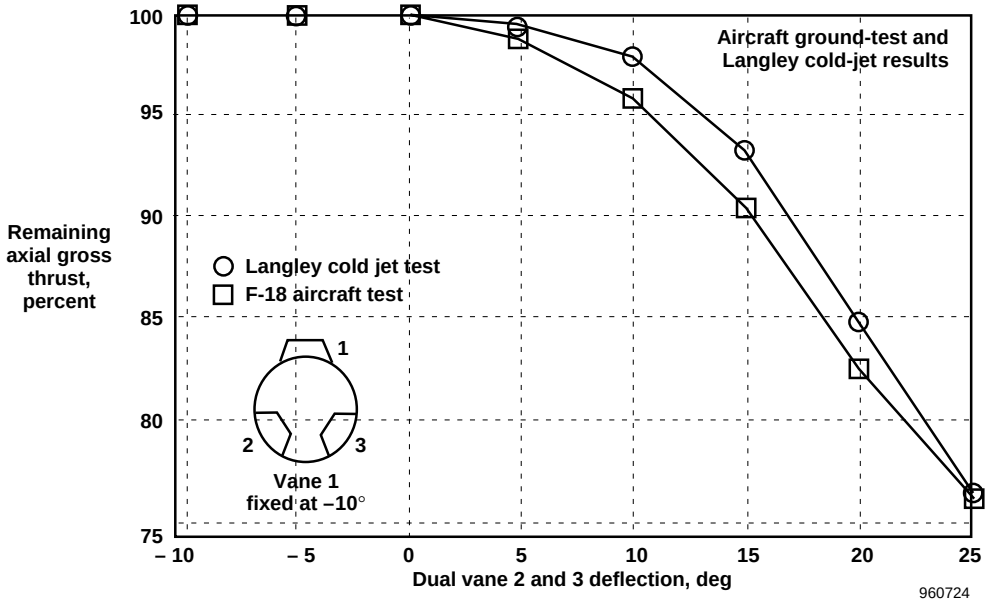

Figure 21. Thrust-vectoring axial force comparison between hot loads thrust-stand and cold-jet test data for vanes 2 and 3 equal deflections.

The cold-jet test data were found to have good correlation of trends with the hot loads test data from thrust vectoring, although the comparison varied in absolute levels with complex jet structures. The infrared results show some promise in being able to characterize thrust-vectoring effectiveness, especially with simple jet structures.

Thrust-Vectoring Flight Tests

Parameter estimation techniques from flight test data produce linearized estimates of stability and control derivatives. Other complications arise because of the mixer of the control law preventing individual vane motions. In this case, an average deflection of the vanes is made based on the measured vane deflections.

In pitch, the upper vanes act in opposition to the lower and outer vanes. A generalized pitch deflection of the vanes is made:

$$dpv = \frac{\left(d1 - \frac{d2 + d3}{2}\right) + \left(d4 - \frac{d5 + d6}{2}\right)}{2} \tag{3}$$

where the vane deflections are defined as follows: *d1* is the upper left vane, *d2* is the outer left vane, *d3* is the lower left vane, *d4* is the upper right vane, *d5* is the outer right vane, and d6 is the lower right vane.

Likewise in yaw, the left vanes of each engine act in opposition to the right vanes of each engine. In this case, the upper vanes do not act strongly in this axis, and deflections of the upper vanes are ignored in yaw. The generalized yaw deflection is then defined as:

$$dyv = \frac{\frac{(d2 - d3)}{2} + \frac{(d6 - d5)}{2}}{2} \tag{4}$$

Estimates of the generalized pitch and yaw deflection vane control power are made in a similar manner. These generalized pitch and yaw control power estimates from the cold-jet test data are used as the baseline to which the flight data are compared. The linearized terms are made from the cold-jet test data in the 15°–20° vane deflection range with military-power nozzle. This range of vane deflections corresponds to the operational area, away from the effects of the plume boundary and nonlinearities near the extreme vectoring envelopes (fig. 12). Referring to the cold-jet test results for single-vane deflections (fig. 7) results in an upper-vane effectiveness of approximately 0.92° of plume deflection for each degree of vane deflection. Doing the same for a two-vane deflection (fig. 10) for the lower and outer vanes gives a slope of approximately 0.97 deg/deg; the generalized average of these is approximately 0.94 deg/deg.

$$C_{dpv} = \frac{\frac{dy}{dx}\,d1 = 20 + \frac{dy}{dx}\,d2, d3 = 20}{\frac{dy}{dx}\,d1 = 15 \qquad d2, d3 = 15}{2} \tag{5}$$

$$C_{dpv} = \frac{0.92 + 0.97}{2} \tag{6}$$

$$C_{dpv} = 0.94 \tag{7}$$

Doing the same in yaw for the lower and outer vanes (fig. 7) requires rotating the axes to the yaw plane by multiplying the cosine of each vane angle to the yaw axis (0.73 and 0.84, respectively) to their slopes of 0.72 deg/deg (the lower and outer vanes are identical in size and control power). Following this procedure, the generalized yaw vane effectiveness of approximately 0.56 deg/deg is found.

$$C_{dyv} = \frac{\left.\frac{dy}{dx}\right|_{dv=15}^{dv=20} \cos(vane\ 2_{angle}) + \left.\frac{dy}{dx}\right|_{dv=15}^{dv=20} \cos(vane\ 3_{angle})}{2} \tag{8}$$

$$C_{dyv} = \frac{0.72\cos(5 + 118 - 90) + 0.84\cos(138.5 - 5 - 90)}{2} \tag{9}$$

$$C_{dyv} = 0.56 \tag{10}$$

In the generalized pitch and yaw effectiveness terms, only the slopes of the control power curves remain. The slopes were relatively insensitive to nozzle size or NPR in the operational region of the vanes (figs. 7 to 9), so these values of vane effectiveness from the cold-jet test data did not vary much for the operating envelope of the aircraft with the engines in military-power to maximum-afterburner settings.

An estimate coefficient was added to the summation of forces and moments equations in the pEst program to model the flight data. The nondimensionalizing parameters for the vane effectiveness coefficients are different than the aerodynamic parameters, so these equations were split into two parts.

$$Normal = \frac{1}{2}\rho v^2 S(C_{N_{aero}}) + F_{np}\left(C_{dpv}\ dpv\right) \tag{11}$$

$$Axial = \frac{1}{2}\rho v^2 S(C_{A_{aero}}) \tag{12}$$

$$pitch = \frac{1}{2}\rho v^2 Sc(C_{m_{aero}}) + F_{np}\ l\left(C_{dpv}\ dpv\right) \tag{13}$$

$$Side = \frac{1}{2}\rho v^2 S(C_{Y_{aero}}) + F_{np}(C_{dyv}\ dyv) \tag{14}$$

$$roll = \frac{1}{2}\rho v^2 Sb(C_l) \tag{15}$$

$$yaw = \frac{1}{2}\rho v^2 Sb(C_{n_{aero}}) + F_{np}\ l(C_{dyv}\ dyv) \tag{16}$$

These summed forces and moments are implemented in the equations of motion just as conventional aerodynamic forces and moments would be added to the equations of motion. An estimate of the net propulsive force, F_{np}, is required for this technique to work, and a simplified gross thrust method was used.[29]

Several maneuvers were executed for parameter identification during the flight test program of the F-18 HARV. Three different sets are examined here: traditional pilot-flown doublets,[21] an optimal programmed set of inputs,[30] and a series of individual doublets commanded to separate control surfaces.[23,26–28] Conventional doublets resulted in excessive levels of correlation between control surfaces, and transient motions were entirely nonexistent. The use of conventional pilot-input doublets, with their large surface correlations, created large Cramer-Rao uncertainty bounds on the estimates and little confidence in the estimates produced. The optimal maneuvers and the series of individual doublets produced low surface correlations with low Cramer-Rao bounds, improving confidence in the estimates produced.

Across the range of angles of attack, little variation was found in the vectoring effectiveness terms (figs. 22 and 23). Uncertainties in the parameter identification estimated thrust-vectoring effectiveness may be from several areas, such as aerodynamic interaction between the thrust vectoring and the external aerodynamics of the F-18 HARV aircraft, possible measurement errors, and residual correlation of control surfaces. The external aerodynamics errors can be thought of as modeling error caused by the model having insufficient degrees of freedom. The residual control surface correlations may be thought of as a deficiency in maneuver design. However, comparison of this vectoring effectiveness, between flight and linearized cold-jet test effectiveness terms, shows an excellent agreement between the two different data sets.

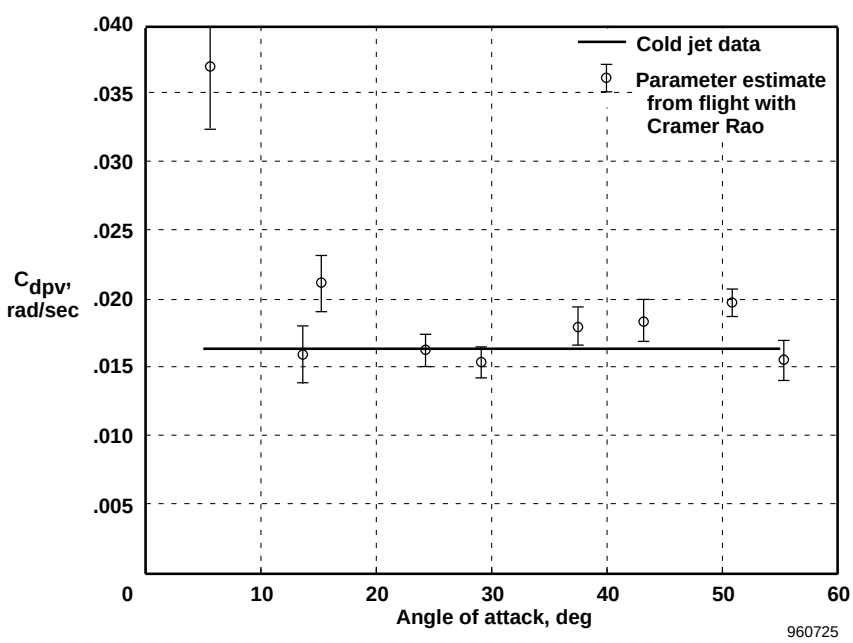

Figure 22. Pitch-vectoring effectiveness comparison between flight data parameter identification estimates and cold-jet test data using vane average positions.

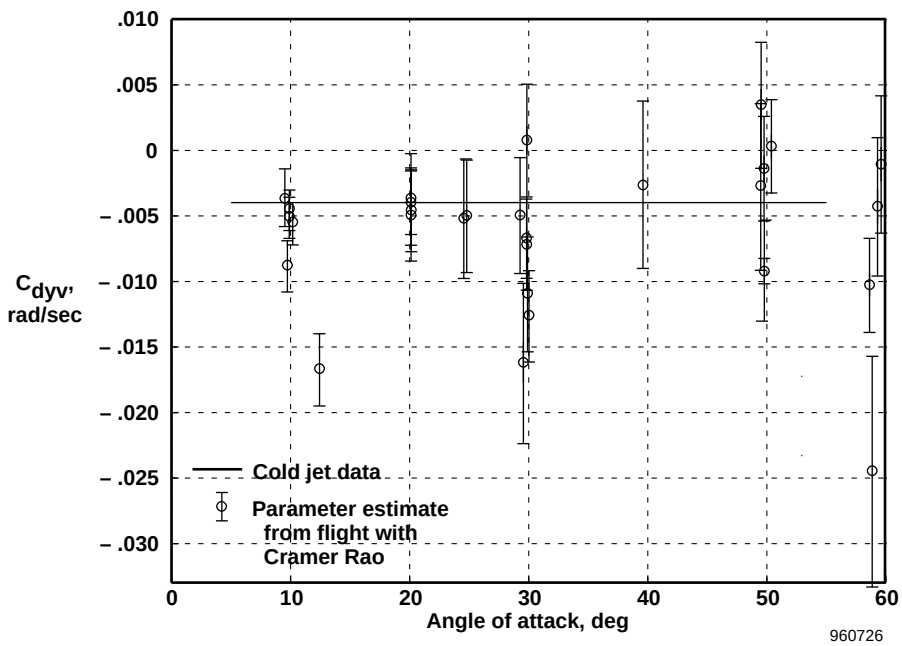

Figure 23. Yaw-vectoring effectiveness comparison between flight data parameter identification estimates and cold-jet test data using vane average positions.

In pitch effectiveness, the parameter identification results show a slight reduction in effectiveness in the 25°–40° angle-of-attack range (fig. 22). Because the pitch effectiveness of the thrust vectoring is independent of angle of attack, little or no sensitivity to this parameter is expected. The slight sensitivity that is found could be caused by the effects of the entrained air around the exhaust plume influencing the aerodynamics around the aircraft, which is a direct result of a modeling error. In addition, it is possible that the large error at low angles of attack in pitch are also caused by aerodynamic interaction. At low angles of attack, the dynamic pressure is elevated in the 1-*g* flight condition, which makes the moment increment caused by aerodynamics large. The results of the cold-jet test data are also shown along with the in-flight estimates, and the correlation is extremely good. The cold-jet test data value of 0.94 deg/deg is also shown. This agreement is extremely good.

In yaw effectiveness, similar results are found with respect to angle of attack in the parameter identification results (fig. 23). A similar reduction in effectiveness, as seen in the pitch effectiveness, is also evident in the yaw effectiveness for the same angle-of-attack region. The yaw vane effectiveness from the cold-jet test data is 0.56 deg/deg, which is also extremely close to the in-flight parameter identification data.

CONCLUDING REMARKS

Data from ground-test investigations and a flight-test investigation of axisymmetric nozzles with postexit vanes that were used to vector the thrust on the NASA F-18 High Alpha Research Vehicle (HARV) aircraft have been presented and compared. Results of these tests

were used to assist in the evaluation of an operational research system that was installed on the NASA F-18 HARV.

Aerodynamic interaction tests were conducted. Aerodynamic interaction test data show the plume deflection to have a mild effect in forces and moments with vectoring. The vectored plume tended to behave similar to a blown flap.

The cold-jet test was used to predict the thrust-vectoring system plume-turning effectiveness. The results of the cold-jet test were that larger vanes are more effective by as much as 50 percent with the maximum-afterburner nozzle, and as much as 25 percent with the military-power nozzle, at a nozzle pressure ratio (NPR) of 2 when compared to the smaller vanes. Increases in NPR (NPR = 6) can result in as much as 5° more turning of the exhaust plume than at lower NPRs (NPR = 2) with the military-power nozzle, although slopes of the vane–to–plume deflection curves were relatively insensitive to NPR. Two-vane equal deflections can produce as much as 100 percent more plume deflection at an NPR of 2 for the military-power nozzle when compared to single-vane deflection results. Military-power nozzle results show slightly more plume-turning control power than maximum-afterburner nozzle results, although slopes are close between the two cases. Axial force loss results from the cold-jet test showed increased losses at increased vane deflections. The vanes are stowed out of the plumes in the –10° deflection position and showed no effectiveness until deflected approximately 10° into the plume for maximum-afterburner and approximately 15° for military-power nozzle at low NPRs.

A ground test of the installed thrust-vectoring system on the F-18 HARV aircraft was conducted. An infrared data technique to measure physical exhaust-plume deflection was used and showed good correlation with the cold-jet test data trends, but also showed mixed results in absolute values. Static-load thrust loss was also measured during this test, and the cold-jet and thrust-stand test data were within 4 percent agreement.

The flight test of thrust-vectoring effectiveness of the vanes was made with parameter identification techniques. Maneuvers were designed and implemented using an on-board excitation system, and pilot-flown maneuvers were analyzed. Because of control system scheduling of the vanes, individual vane effectiveness could not be directly measured, but overall combined effects could be compared between the cold-jet and flight test data. Flight data estimates of pitch-vectoring effectiveness show approximately 0.9° plume deflection for each degree generalized pitch vane deflection, and 0.6° plume deflection for each degree of generalized yaw vane deflection in yaw. This pitch and yaw vane effectiveness showed extremely good correlation between cold-jet test data and flight parameter identification techniques.

REFERENCES

[1]Chambers, Joseph R. “High-Angle-of-Attack Technology: Progress and Challenges,” *High-Angle-of-Attack Technology*, NASA CP-3149, vol. 1, May 1992, pp. 1–22.

[2]Chambers, J. R., “High-Angle-of-Attack Aerodynamics: Lessons Learned,” AIAA-86-1774, June 1986.

[3]Berrier, B. L. and Leavitt, L. D., *Static Internal Performance of Single-Expansion-Ramp Nozzles With Thrust-Vectoring Capability up to 60°*, NASA TP-2364, Oct. 1984.

[4]Murri, Daniel G., Grafton, Sue B., and Hoffler, Keith D., *Wind Tunnel Investigation and Free-Flight Evaluation of a Model of the F-15 STOL and Maneuver Technology Demonstrator*, NASA TP-3003, Aug. 1990.

[5]Sappington, Jeffery W. and Thompson, Robert L., "F-14A Yaw Vane Technology Demonstration Program," *Society of Experimental Test Pilots 31st Symposium Proceedings*, Sept., 1987, pp. 187–200.

[6]Mason, M. L. and Berrier, B. L., *Static Investigation of Several Yaw Vectoring Concepts on Nonaxisymmetric Nozzles*, NASA TP-2432, June 1985.

[7]Mason, Mary L. and Berrier, Bobby L., *Static Performance of Nonaxisymmetric Nozzles With Yaw Thrust-Vectoring Vanes*, NASA TP-2813, May 1988.

[8]Berrier, Bobby L. and Mason, Mary L., *Static Performance of an Axisymmetric Nozzle With Post-Exit Vanes for Multiaxis Thrust Vectoring*, NASA TP-2800, May 1988.

[9]Capone, F. J. and Mason, M. L., *Multiaxis Aircraft Control Power From Thrust Vectoring at High Angles of Attack*, NASA TM-87741, June 1986.

[10]Capone, F. J. and Berrier, B. L., *Investigation of Axisymmetric and Nonaxisymmetric Nozzles Installed on a 0.10-Scale F-18 Prototype Airplane Model*, NASA TP-1638, June 1980.

[11]Tamrat, B. F. and Antani, D. L., "Static Test Results of an Externally Mounted Thrust Vectoring Vane Concept," AIAA-88-3221, July 1988.

[12]Regenie, Victoria, Gatlin, Donald, Kempel, Robert, and Matheny, Neil, "The F-18 High Alpha Research Vehicle: A High-Angle-of-Attack Testbed Aircraft," AIAA-92-4121, Aug. 1992.

[13]Gera, Joseph, "Flight Test Status of the NASA High-Angle-of-Attack Technology Program," *High-Angle-of-Attack Projects and Technology Conference*, NASA CP-3137, vol. 2, Apr. 1992.

[14]Kempel, Robert, *F-18 High Alpha Research Vehicle Description*, Uniform Resource Locater http://www.dfrc.nasa.gov/Projects/HARV/VDD/kempel2.html

[15]Bowers, Albion H., Regenie, Victoria A., and Flick, Bradley C., "F-18 High Alpha Research Vehicle: Lessons Learned," *Fourth High Alpha Conference*, NASA CP-10143, vol. 2, July 1994.

[16]Bowers, Albion H., Noffz, Gregory K., Grafton, Sue B., Mason, Mary L., and Peron, Lee R., *Multiaxis Thrust Vectoring Using Axisymmetric Nozzles and Postexit Vanes on an F/A-18 Configuration Vehicle*, NASA TM-101741, Apr. 1991.

[17]Asbury, Scott C. and Capone, Francis J., *Multiaxis Thrust-Vectoring Characteristics of a Model Representative of the F-18 High-Alpha Research Vehicle at Angles of Attack From 0° to 70°*, NASA TP-3531, Dec. 1995.

[18]Mason, Mary L., Capone, Francis J., and Asbury, Scott C., *A Static Investigation of the Thrust Vectoring System of the F/A-18 High-Alpha Research Vehicle*, NASA TM-4359, June 1992.

[19]Johnson, Steven A., *Aircraft Ground Test and Subscale Model Results of Axial Thrust Loss Caused by Thrust Vectoring Using Turning Vanes*, NASA TM-4341, Jan. 1992.

[20]Maine, Richard E. and Iliff, Kenneth W., *Identification of Dynamic Systems: Theory and Formulation*, NASA RP-1138, Feb. 1985.

[21]Maine, Richard E. and Iliff, Kenneth W., *Application of Parameter Estimation to Aircraft Stability and Control: The Output-Error Approach*, NASA RP-1168, June 1986.

[22]Murray, James E. and Maine, Richard E., *pEst Version 2.1 User's Manual*, NASA TM-88280, Sept. 1987.

[23]Gates, Russell J., Bowers, Albion H., and Howard, Richard M., "A Comparison of Flight Input Techniques for Parameter Estimation of Highly-Augmented Aircraft," *AIAA Atmospheric Flight Mechanics Conference*, AIAA-96-3363-CP, July 1996, pp. 31–38.

[24]Pahle, Joseph W., Powers, Bruce, Regenie, Victoria, Chacon, Vince, Degroote, Steve, and Murnyak, Steven, *Research Flight-Control System Development for the F-18 High Alpha Research Vehicle*, NASA TM-104232, Apr. 1991.

[25]Bundick, W. T., Pahle, J. W., Yeager, J. C., and Beissner, F. L., Jr., *Design of a Mixer for the Thrust-Vectoring System on the High-Alpha Research Vehicle*, NASA TM-110228, June 1996.

[26]Napolitano, Marcello R., Paris, Alfonso C., Spagnuolo, Joelle, and Bowers, Albion H., "Parameter Estimation for the NASA F/A-18 HARV at High Angles of Attack," *AIAA Atmospheric Flight Mechanics Conference*, AIAA-94-3504-CP, Aug. 1994, pp. 388–398.

[27]Napolitano, Marcello R., Paris, Alfonso C., Seanor, Brad A., and Bowers, Albion H., "Estimation of the Lateral-Directional Aerodynamic Parameters from Flight Data for the NASA F/A-18 HARV," *AIAA Atmospheric Flight Mechanics Conference*, AIAA-96-3420-CP, July 1996, pp. 479–489.

[28]Napolitano, Marcello R., Paris, Alfonso C., Seanor, Brad A., and Bowers, Albion H., "Estimation of the Longitudinal Aerodynamic Parameters from Flight Data for the NASA F/A-18 HARV," *AIAA Atmospheric Flight Mechanics Conference*, AIAA-96-3419-CP, July 1996, pp. 469–478.

[29]Ray, Ronald J., *Evaluation of Various Thrust Calculation Techniques on an F404 Engine*, NASA TP-3001, Apr. 1990.

[30]Morelli, Eugene A., "Flight Test Validation of Optimal Input Design Using Pilot Implementation," IFAC SYSID-No. 559, July 1994.

REPORT DOCUMENTATION PAGE

Form Approved
OMB No. 0704-0188

Public reporting burden for this collection of information is estimated to average 1 hour per response, including the time for reviewing instructions, searching existing data sources, gathering and maintaining the data needed, and completing and reviewing the collection of information. Send comments regarding this burden estimate or any other aspect of this collection of information, including suggestions for reducing this burden, to Washington Headquarters Services, Directorate for Information Operations and Reports, 1215 Jefferson Davis Highway, Suite 1204, Arlington, VA 22202-4302, and to the Office of Management and Budget, Paperwork Reduction Project (0704-0188), Washington, DC 20503.

1. AGENCY USE ONLY (Leave blank)

2. REPORT DATE
November 1996

3. REPORT TYPE AND DATES COVERED
Technical Memorandum

4. TITLE AND SUBTITLE
Thrust Vectoring on the NASA F-18 High Alpha Research Vehicle

5. FUNDING NUMBERS
WU 505-68-30

6. AUTHOR(S)
Albion H. Bowers and Joseph W. Pahle

7. PERFORMING ORGANIZATION NAME(S) AND ADDRESS(ES)
NASA Dryden Flight Research Center
P.O. Box 273
Edwards, California 93523-0273

8. PERFORMING ORGANIZATION REPORT NUMBER
H-2139

9. SPONSORING/MONITORING AGENCY NAME(S) AND ADDRESS(ES)
National Aeronautics and Space Administration
Washington, DC 20546-0001

10. SPONSORING/MONITORING AGENCY REPORT NUMBER
NASA TM-4771

11. SUPPLEMENTARY NOTES
Presented at the NASA Langley High-Angle-of-Attack Technology Conference, Langley Research Center, Hampton, Virginia, Sept. 17–19, 1996. Albion H. Bowers and Joseph W. Pahle, NASA Dryden Flight Research Center, Edwards, California.

12a. DISTRIBUTION/AVAILABILITY STATEMENT
Unclassified—Unlimited
Subject Category 20

12b. DISTRIBUTION CODE

13. ABSTRACT (Maximum 200 words)

Investigations into a multiaxis thrust-vectoring system have been conducted on an F-18 configuration. These investigations include ground-based scale-model tests, ground-based full-scale testing, and flight testing. This thrust-vectoring system has been tested on the NASA F-18 High Alpha Research Vehicle (HARV). The system provides thrust vectoring in pitch and yaw axes. Ground-based subscale test data have been gathered as background to the flight phase of the program. Tests investigated aerodynamic interaction and vane control effectiveness. The ground-based full-scale data were gathered from static engine runs with image analysis to determine relative thrust-vectoring effectiveness. Flight tests have been conducted at the NASA Dryden Flight Research Center. Parameter identification input techniques have been developed. Individual vanes were not directly controlled because of a mixer-predictor function built into the flight control laws. Combined effects of the vanes have been measured in flight and compared to combined effects of the vanes as predicted by the cold-jet test data. Very good agreement has been found in the linearized effectiveness derivatives.

14. SUBJECT TERMS
Aircraft parameter identification, Cold jet testing, Flight test, Thrust vectoring, Wind tunnel testing

15. NUMBER OF PAGES
32

16. PRICE CODE
AO3

17. SECURITY CLASSIFICATION OF REPORT
Unclassified

18. SECURITY CLASSIFICATION OF THIS PAGE
Unclassified

19. SECURITY CLASSIFICATION OF ABSTRACT
Unclassified

20. LIMITATION OF ABSTRACT
Unlimited